G.A. Akopdzhanov, V.B. Anikeev, V.A. Bezzubov,
S.P. Denisov, A.A. Durum, Yu.V. Gilitsky, S.N. Gurzhiev,
V.M. Korablev, V.I. Koreshev, A.V Kozelov [1], E.A. Kozlovsky,
V.I. Kurbakov, V.V. Lipaev, V.A. Onuchin, A.M. Rybin,
Yu.M. Sapunov, A.A. Schukin, M.M. Soldatov,
D.A. Stoyanova, K.I. Trushin, I.A. Vasilyev, V.I. Yakimchuk,
S.A. Zvyagintsev

State Research Center Institute for High Energy Physics, Protvino, Moscow oblast, 142281 Russia

Measurements of the Charge Asymmetry of the Dalitz Plot Parameters for $K^{\pm} \to \pi^{\pm}\pi^0\pi^0$ Decays

Abstract

The charge asymmetry of the g, h, and k Dalitz plot parameters for $K^{\pm} \to \pi^{\pm}\pi^0\pi^0$ decays has been measured with 35 GeV/c hadron beams at the 70 GeV IHEP accelerator. The g, h, and k values obtained appear to be identical for $K^{\pm}$ decays within the errors quoted. In particular, the charge asymmetry $A_g = (g^+ - g^-)/(g^+ + g^-)$ of the slope g is equal to $(0.2 \pm 1.9) \cdot 10^{-3}$.

1 INTRODUCTION

Observation of direct CP violation in neutral kaon decays [1,2,3] gives arguments to search for a similar effect in charged kaon decays. For example, this effect can manifest itself as a charge asymmetry of the Dalitz plot parameters for $K^{\pm} \to \pi^{\pm}\pi^0\pi^0$ decays. These parameters are coefficients in a series expansion of the squared module of the matrix element [4]:

$$|M(u,v)|^2 \propto 1 + gu + hu^2 + kv^2, \quad (1)$$

[1] Corresponding author. *E-mail address:* kozelov@mx.ihep.su

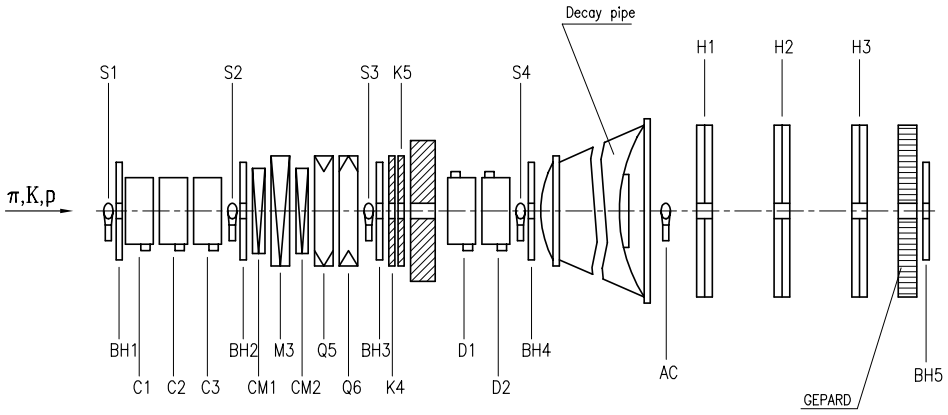

Fig. 1. Experimental layout: M – magnets, Q – quadrupoles, CM – tuning magnets, K – collimators, S – scintillation counters, C,D – threshold and differential Čherenkov counters, BH – beam hodoscopes, AC – anticoincidence counter, H – scintillation hodoscopes, GEPARD – electromagnetic calorimeter.

where u and v are invariant variables.

Theoretical estimates of the charge asymmetry of the Dalitz plot slope g for $K^{\pm} \to \pi^{\pm}\pi^0\pi^0$ decays are uncertain and range from 10^{-6} to 10^{-3} [5,6,7,8]. In the majority of the experiments, only g^+ or g^- was measured [4,9]. From these studies it follows that $\Delta g = g^+ - g^- = 0.066 \pm 0.017$. It is very unlikely to expect direct CP violation at this level, and one can assume that the above mentioned difference is due to the underestimation of the systematic uncertainties.

$K \to 3\pi$ decays have been studied simultaneously for both K^+ and K^- mesons in [10,11,12]. Ford *et al.* [10] found $A_g = -0.0070 \pm 0.0053$ for $K^{\pm} \to \pi^{\pm}\pi^{\pm}\pi^{\mp}$ decays. In the experiment [11], $A_g = 0.0019 \pm 0.0123$ was measured for $K^{\pm} \to \pi^{\pm}\pi^0\pi^0$ decays. Preliminary analysis of our experimental data [12] based on a fraction of statistics yielded $A_g = -0.0003$ with a statistical error of 0.0025 and a systematical uncertainty below 0.0015. In this paper we report our final results on the charge asymmetry of the Dalitz plot parameter measurements.

2 EXPERIMENTAL SETUP

The experiment was carried out with the TNF-IHEP facility [13] (Fig. 1) at the 70 GeV IHEP accelerator. Unseparated 35 GeV/c positive and negative hadron beams used for kaon decay studies are produced by 70 GeV protons in the external 30 cm Al target. Scintillation counters S1-S4 and beam hodoscopes BH1-BH4 are used to monitor beam intensity and to measure particle trajectories and beam profiles. The typical particle flux was $4{\times}10^6$ per 1.7 second spill.

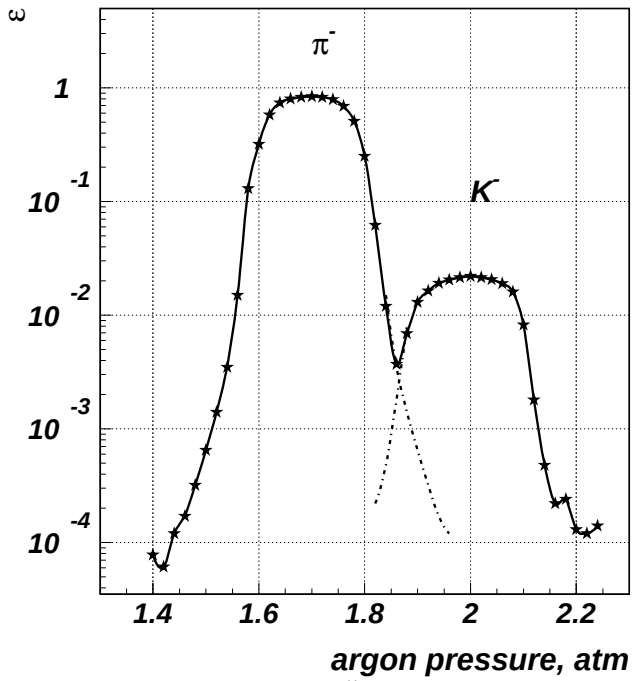

Fig. 2. Efficiency of the differential Čherenkov counters vs argon pressure.

Kaons are selected with three threshold C1-C3 and two differential D1, D2 gas Čherenkov counters (Fig. 1). The admixture of unwanted particles under the kaon peak was substantially below 1% (Fig. 2). The threshold counters are also used to select 10 GeV/c electrons to calibrate GEPARD calorimeter.

About 20% of kaons decay in the 58.5 m long vacuum pipe located downstream of the BH4 hodoscope. The flanges of the vacuum pipe have thin Mylar windows in the path of beam particles. The 3.6 m diameter exit flange is made of 4 mm thick (0.23 X_0) stainless steel. The probability of a high-energy photon to convert into an e^+e^- pair in this flange is equal to 0.16.

Kaons which pass through the decay pipe are detected by the anticoincidence counter AC. The BH5 beam hodoscope placed behind the calorimeter is used for a high precision measurement of the beam position at the setup end. The BH5 hodoscope operates in the counting mode and hence detects all beam particles.

The products of kaon decays are detected by three scintillation hodoscopes H1-H3 [14] and the GEPARD electromagnetic calorimeter. Each hodoscope is made of two X,Y octagonal planes with 3.85 m distance between the opposite octagonal sides (Fig. 3). The plane is divided into half-planes with 256 elements each. The cross section of the hodoscope elements is 14×12 mm^2 and their length varies from 0.7 to 1.8 m. Scintillation light is detected by FEU-84-3 photomultiplier tubes.

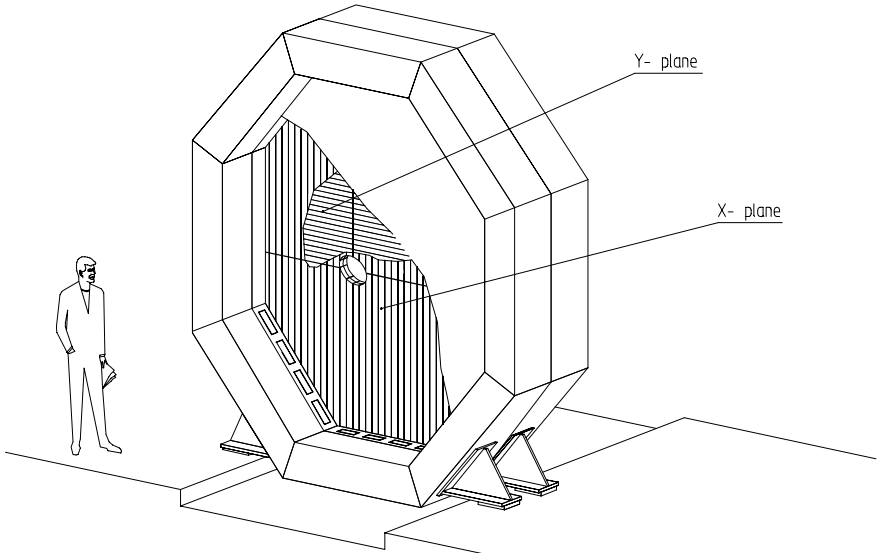

Fig. 3. General view of the scintillation hodoscope H.

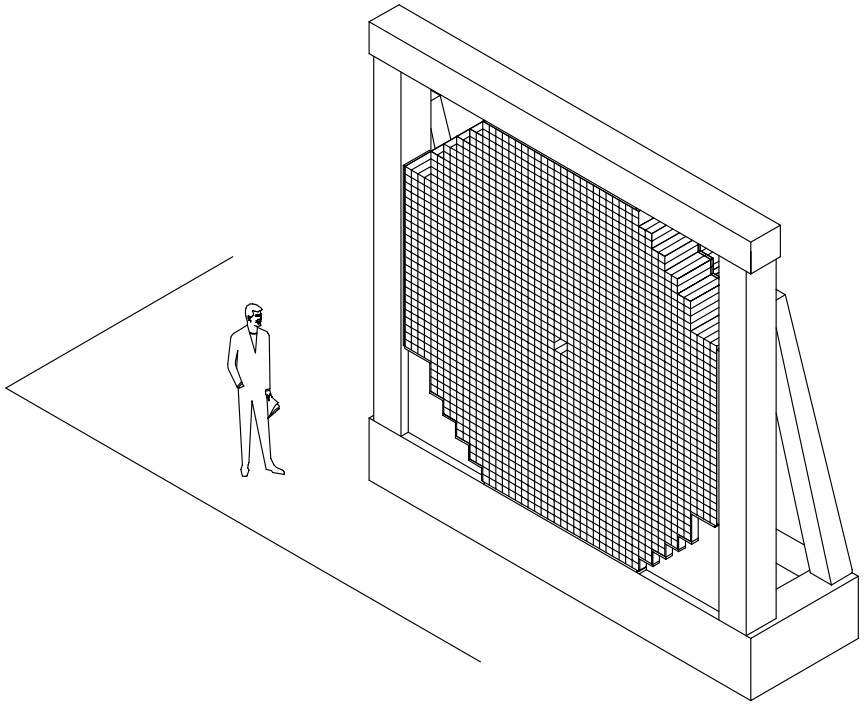

Fig. 4. The GEPARD calorimeter.

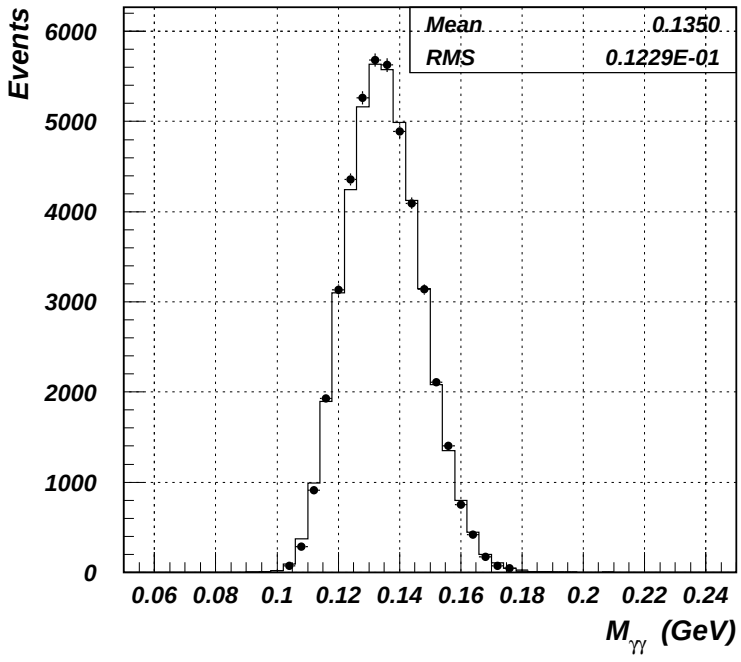

Fig. 5. $M_{\gamma\gamma}$ distribution for $K^{\pm} \to \pi^{\pm}\pi^0$ decays.

The GEPARD is a sampling lead-scintillator calorimeter. It contains 1968 cells with 76×76 mm^2 cross section (Fig. 4). Each cell consists of 40 alternating layers of 3 mm Pb and 5 mm scintillator. The total radiation length is 21 X_0. Scintillation light is collected onto FEU-84-3 photomultiplier tubes using wavelength shifting light guides. The GEPARD calorimeter was calibrated by irradiating each cell with 10 GeV/c electrons at the beginning of data taking and by using $K^{\pm} \to \pi^{\pm}\pi^0$ reconstructed events collected during the experiment. Both methods yielded consistent results. The π^0 mass resolution is equal to 12.3 MeV/c^2 (Fig. 5).

The Level 1 trigger is formed according to the logic formula

$$T1 = S1 \cdot S2 \cdot S3 \cdot S4 \cdot (D1 + D2) \cdot \overline{C1} \cdot \overline{C2} \cdot \overline{C3} \cdot \overline{AC}.$$

The Level 2 trigger uses information about energy deposition in the GEPARD calorimeter [15]. For this purpose the calorimeter is divided into 16 trigger elements. The Level 2 trigger is formed if the energy deposition exceeds 0.8 GeV in at least three trigger channels.

The stability of the beam and detector parameters was carefully monitored during the data collection. To reduce the systematical uncertainty in the measurement of the charge asymmetry of the Dalitz plot parameters the beam polarity was reversed every day. Figs. 6-7 illustrate the stability of the experimental setup operation.

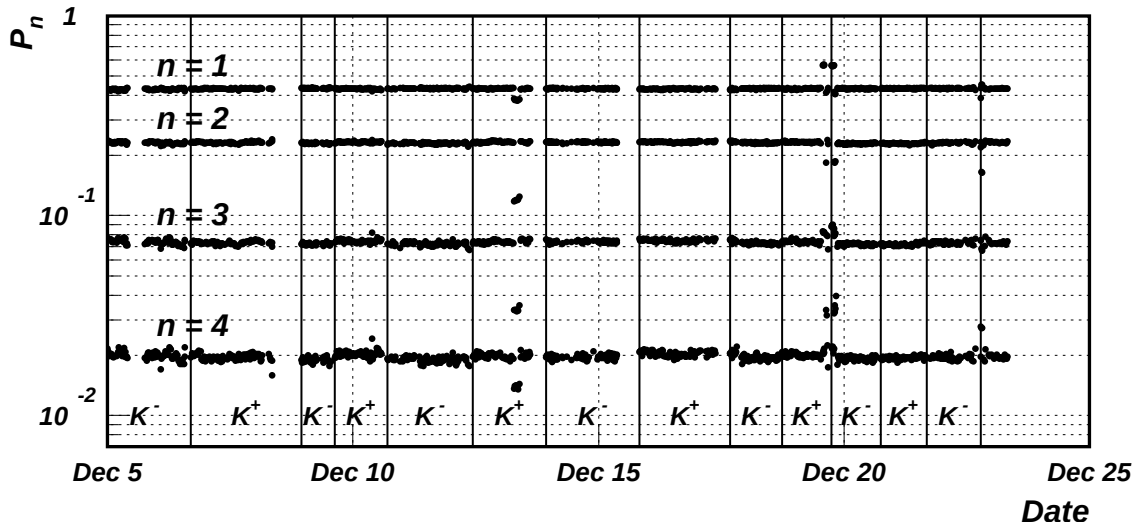

Fig. 6. Time variations of the probability P_n to reconstruct n tracks (P_n is averaged over $\sim 10^5$ events).

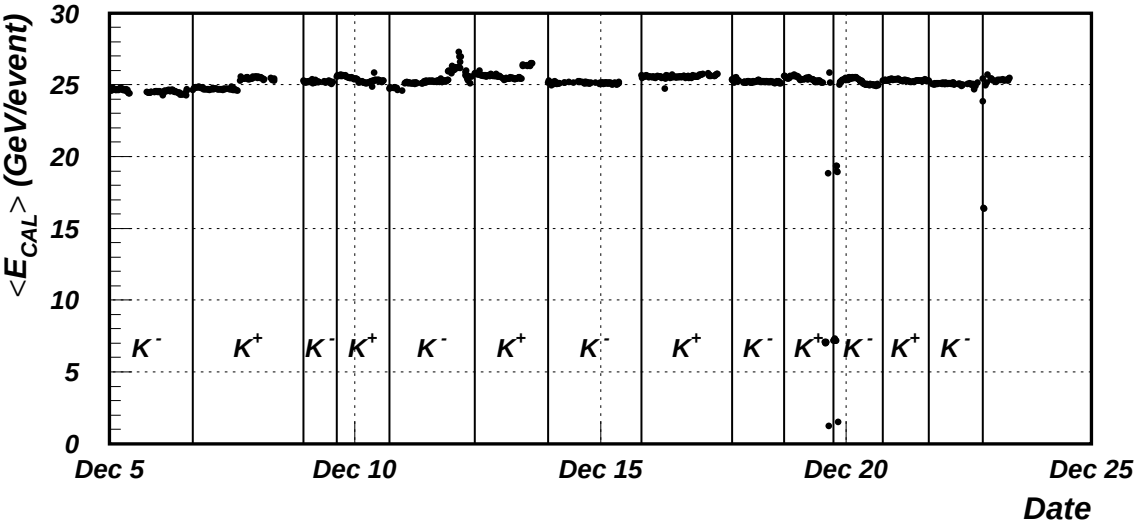

Fig. 7. Time variation of the mean energy per event detected in the GEPARD calorimeter (E_{Cal} is averaged over $\sim 10^5$ events).

3 EVENT RECONSTRUCTION AND SELECTION CRITERIA

The $K^{\pm} \to \pi^{\pm}\pi^0\pi^0$ event selection starts by finding energy clusters in the GEPARD calorimeter. The coordinates of the cluster centers and the X and Y coordinates measured by H1–H3 hodoscopes are used in track reconstruction. To reduce the combinatorial background, only tracks with three or four hits in each X and Y projection are selected. Then the vertex position of the $K^{\pm}$ decay is calculated using the reconstructed tracks. A track is considered to be associated with a kaon decay if the hypothesis of its intersection with beam axis has a confidence level of 5% or more and the decay vertex position is

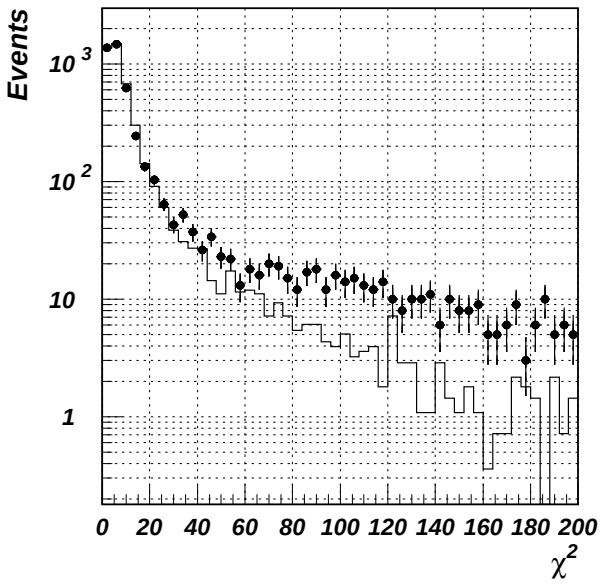

Fig. 8. χ^2 distribution for $K^{\pm} \to \pi^{\pm}\pi^0\pi^0$ decays (histogram – simulation, circles – experiment).

inside the fiducial volume of the decay pipe. In addition selected events have to satisfy one of the following criteria:

- five clusters with energies above 1 GeV are found and each track is associated with one of these clusters;
- four clusters with energies above 1 GeV are found and one of the tracks is not associated with these clusters.

These criteria are applied because there is a substantial probability for the gamma from π^0 decays to convert into e^+e^- pair in the exit flange of the decay pipe (see Section 2), and charged pion energy deposition in the calorimeter could exceed the threshold value of 1 GeV.

Events passing this preliminary selection are subjected to a kinematic fit that allows one to resolve ambiguities due to the combinatorial background (for example, to associate one of the tracks with the charged pion) and to calculate the Dalitz plot variables. Altogether 21 measured parameters are used in the fitting procedure: the energies and the coordinates of four clusters associated with gammas, the kaon mean energy and the parameters of the kaon and pion tracks. The parameters of the clusters are corrected for the transverse profile of the electromagnetic shower and for the spatial nonuniformity of the calorimeter. The energy of the charged pion is the only unknown parameter.

Seven constraints are imposed on the fitted parameters: four equations of the energy-momentum conservation, two equations for the effective masses of the gamma pairs and a required intersection of kaon and charged pion trajectories. The decay vertex coordinates are not fixed. The parameters are found by the

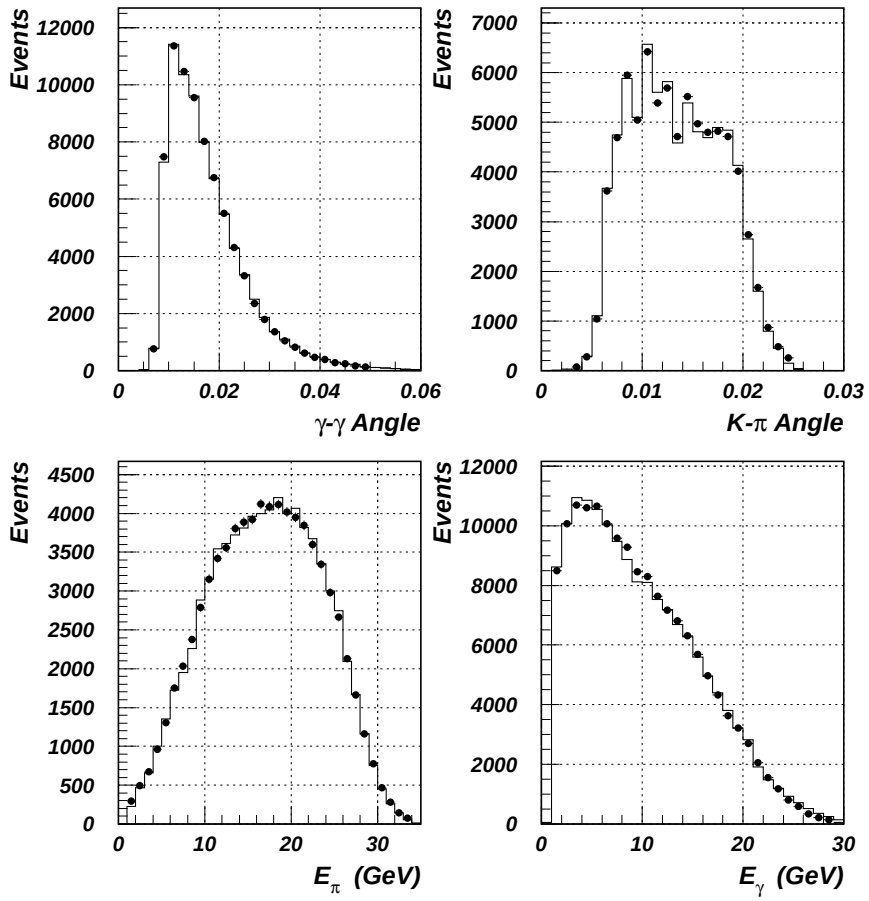

Fig. 9. Number of events vs kinematic variables for $K^\pm \to \pi^\pm\pi^0$ decays (histogram – simulation, circles – experiment).

minimization of the functional with constraints using the method of uncertain Lagrange multipliers and iteration technique. The iterations are stopped when the relative changes of all fitted parameters at the last iteration are less than 10^{-5}. For each event all possibilities to associate one of the tracks with charged pion and γ pairs with π^0's are considered. The combination with the least χ^2 is used. Fig. 8 shows the χ^2 distributions for the data and simulated events. Events with $\chi^2 > 20$ are rejected since in this region the data exceeds the number of the simulated events due to the high background level. Simulation shows that this χ^2 cut reduces statistics of the wanted events by 28% only but decreases background level considerably.

The experimental setup operation was simulated using a Monte Carlo (MC) method with the GEANT 3.21 code. The setup geometry is described in de-

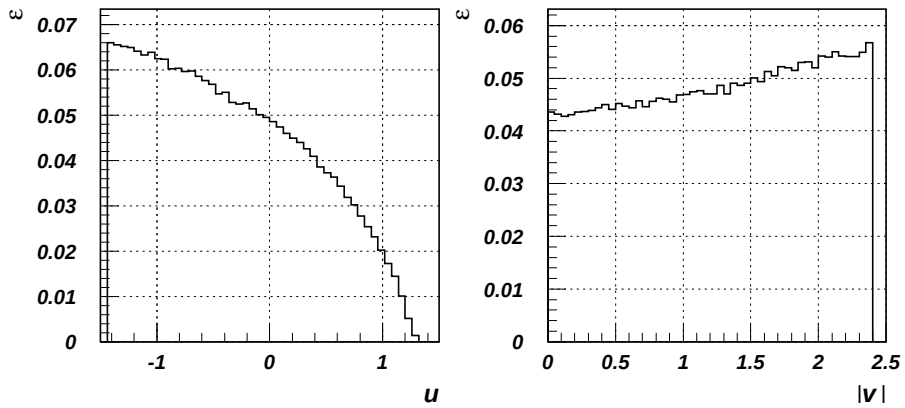

Fig. 10. Acceptance vs Dalitz plot variables.

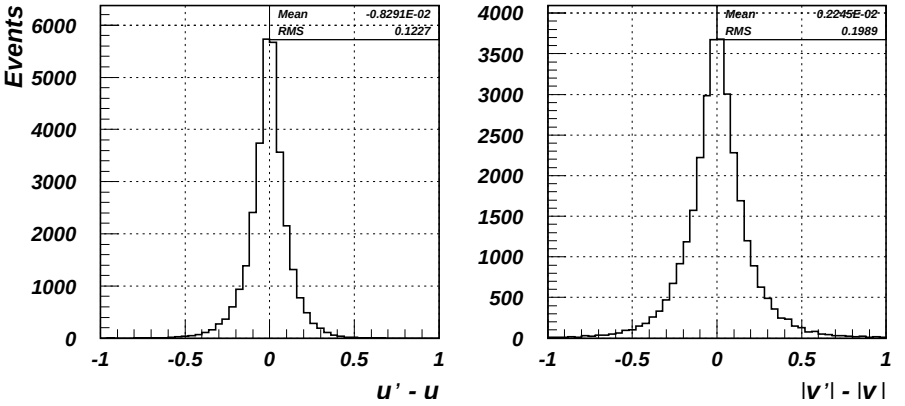

Fig. 11. u, v resolutions (u, v – "true" variables, u', v' – measured variables).

tail, and the data obtained in the experiment were taken into account. Among these data are the calibration coefficients for each channel of the calorimeter, the dependence of the hodoscope efficiency on the particle coordinates and correlations between kaon spatial and angular coordinates and its momentum. Fig. 9 presents different distributions of the experimental data and simulated events for the $K^{\pm} \to \pi^{\pm}\pi^0$ decays. From this figure it follows that there is a good agreement between experimental and simulated distributions. Fig. 10 shows the acceptance of the setup, and Fig. 11 demonstrates the u, v resolutions averaged over the Dalitz plot.

The χ^2 probability $P(\chi^2)$ for data and simulation is shown in Fig. 12. Events with $P(\chi^2) > 0.1$ are selected for further analysis since in this region there is a good agreement between the experimental and simulated data. To check the Level 2 trigger conditions the energies corresponding to each of the trigger channels are calculated. The event is accepted if the number of the channels with energy above 1 GeV is greater than two. This cut rejects only a few $K^{\pm} \to \pi^{\pm}\pi^0\pi^0$ events (see the last row of Table 1), but it is important for $K^{\pm} \to \pi^{\pm}\pi^0$ event selection which is used to calibrate the calorimeter, to adjust the simulation code, and to estimate the systematic uncertainties.

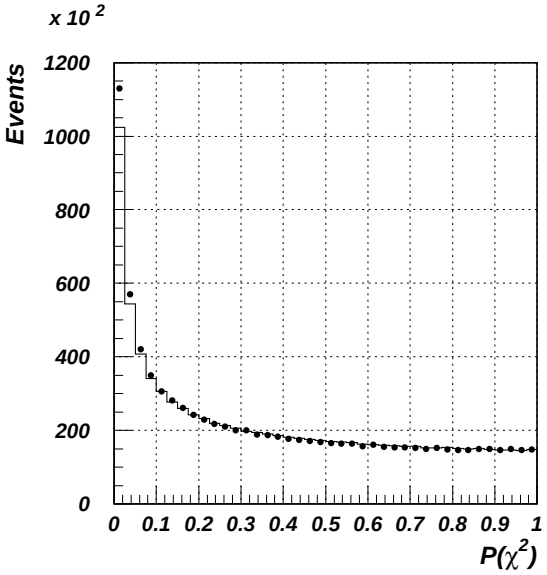

Fig. 12. $P(\chi^2)$ distribution for $K^{\pm} \to \pi^{\pm}\pi^0\pi^0$ decays (histogram – simulation, circles – experiment).

The final data sample is comprised of $N^+ = 278398$ and $N^- = 341015$ events. Table 1 shows the fraction of events rejected by each cut and the cumulative efficiency.

Table 1

Selection criteria	Fraction (%) of events	
	rejected by the cut	passed this and all previous cuts
≥ 1 track is reconstructed in H1-H3	4.4	95.6
Position of the decay vertex is inside the fiducial length of the decay pipe	31.2	65.7
Number of clusters and tracks corresponds to the $K^{\pm} \to \pi^{\pm}\pi^0\pi^0$ decay	93.2	4.48
$\chi^2 < 20$	82.2	0.80
$P(\chi^2) > 0.1$	26.4	0.59
Level 2 trigger is ok	0.2	0.59

After all selection cuts for $K^{\pm} \to \pi^{\pm}\pi^0\pi^0$ decays, an admixture of background remains. The background sources are other modes of kaon decays, interactions of beam particles in the material along the beam line and overlapping of events due to the finite time resolution of the detectors. Simulations of these processes demonstrate that the main contribution to the background comes from the

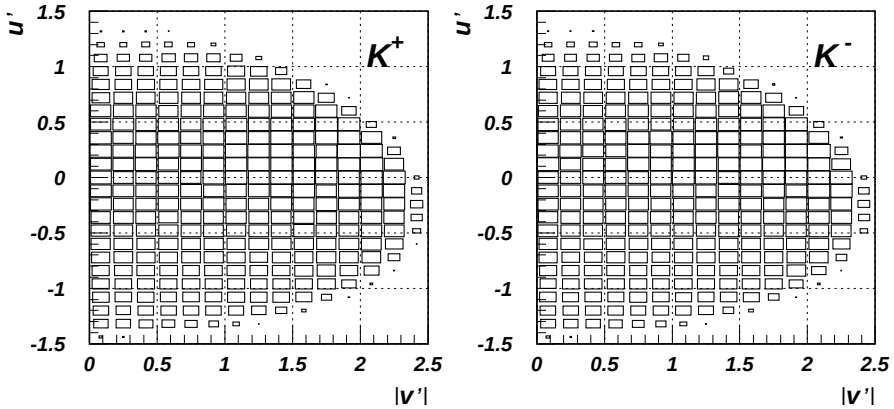

Fig. 13. Distribution of events in the Dalitz plots for $K^{\pm} \to \pi^{\pm}\pi^0\pi^0$ decays.

$K^{\pm} \to \pi^{\pm}\pi^0$ (0.21%) and $K^{\pm} \to \pi^{\pm}\pi^+\pi^-$ (0.03%) decays. This contribution does not depend on the sign of the kaon charge and hence does not cause a false charge asymmetry of the Dalitz plots. The background level from other sources is less than 0.01%.

The finite energy resolution of the calorimeter results in a noticeable ($\sim 10\%$) probability of the wrong combinations of γ's reconstructed into π^0's and the hodoscope inefficiency can cause a reconstruction of a false track ($\sim 5\%$). Both these effects are taken into account in the event simulation and it is found that their influence on the charge asymmetry of the Dalitz plot parameters is negligible.

4 RESULTS

4.1 Difference of the Dalitz plot parameters

The difference of the Dalitz plot parameters for $K^{\pm}$ decays is estimated by minimizing the following functional form:

$$\chi^2(\Delta g, \Delta h, \Delta k) = \sum_{i,j} \frac{(r_{ij} - 1 - \alpha_{ij}\Delta g - \beta_{ij}\Delta h - \gamma_{ij}\Delta k)^2}{\sigma_{ij}^2}, \qquad (2)$$

$r_{ij} = \frac{n^+_{ij}/N^+}{n^-_{ij}/N^-}$, $\sigma^2_{ij} = r^2_{ij} \cdot \left(\frac{1}{n^+_{ij}} + \frac{1}{n^-_{ij}}\right)$, where $n^{\pm}_{ij}$ is the number of events in the i-th, j-th Dalitz plot bin with u', v' measured coordinates (Fig. 13), and α_{ij}, β_{ij}, and γ_{ij} are coefficients defined in (A.2) (see Appendix) and calculated by MC. The values of Δg, Δh, and Δk as well as the elements of the correlation

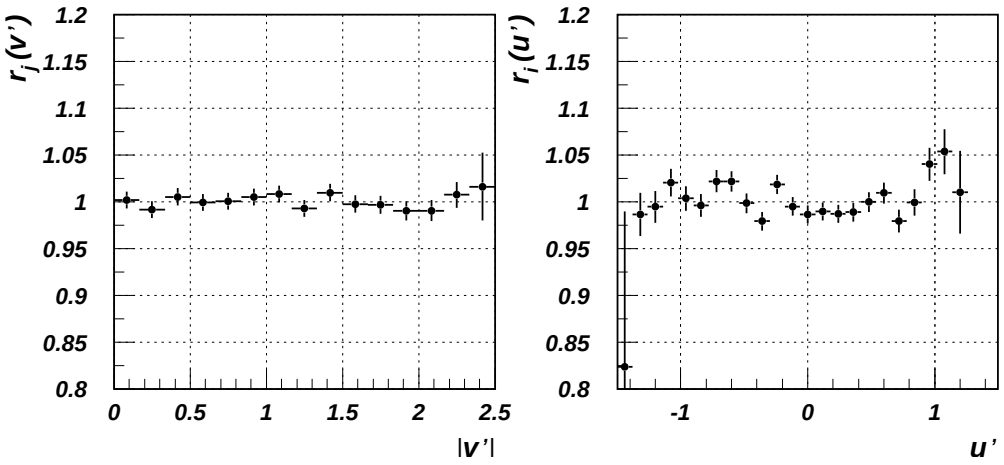

Fig. 14. Ratios of normalized event distributions projected on the u' and $|v'|$ axes.

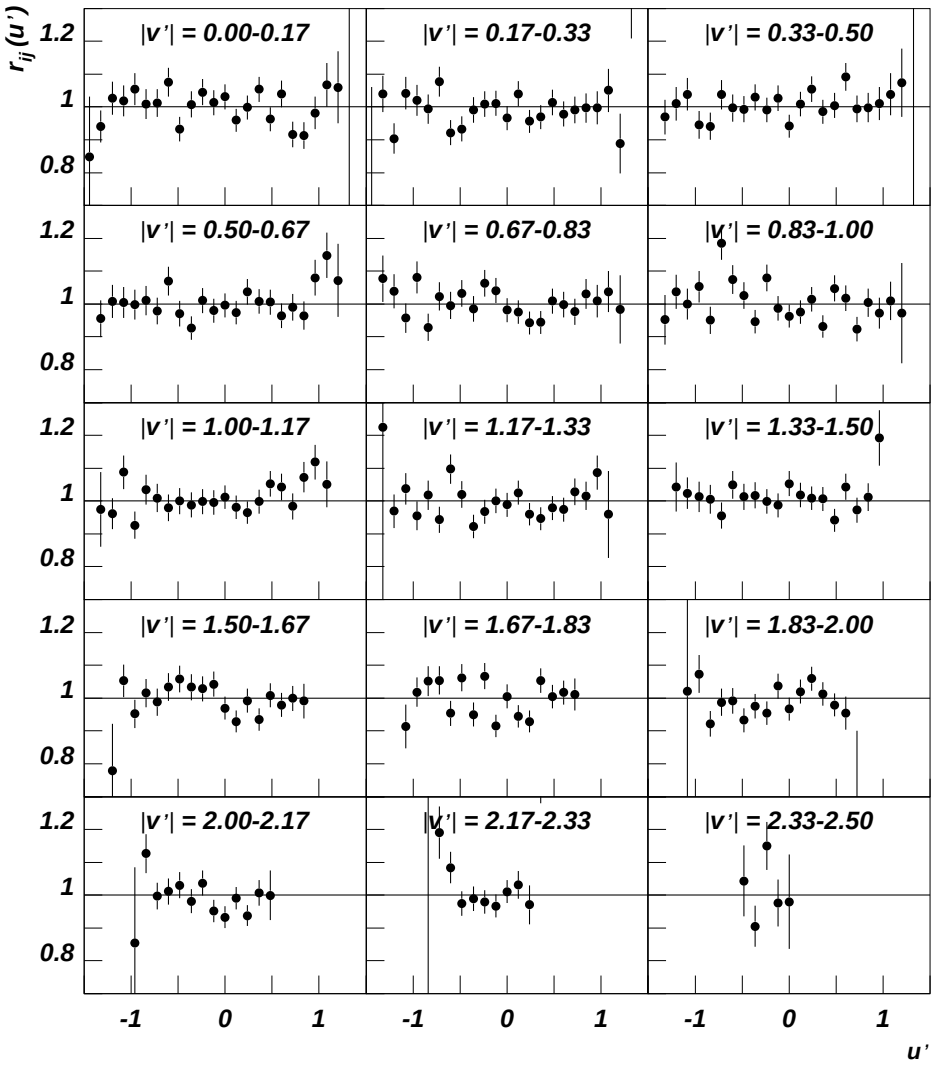

Fig. 15. Ratios of normalized event distribution vs u' for the different $|v'|$ intervals.

matrix are given in (3):

$$\begin{cases} \Delta g = -0.0009 \pm 0.0067, \\ \Delta h = -0.0007 \pm 0.0062, \\ \Delta k = -0.0014 \pm 0.0017, \end{cases} \qquad \begin{pmatrix} 1.00 & 0.93 & 0.35 \\ & 1.00 & 0.32 \\ & & 1.00 \end{pmatrix} \tag{3}$$

The errors shown are statistical only. The χ^2/ndf is 319/(279-3) = 1.16.

Fig. 14 shows the $r_i(u') = \frac{\sum\limits_j n^+_{ij}/N^+}{\sum\limits_j n^-_{ij}/N^-}$ and $r_j(v') = \frac{\sum\limits_i n^+_{ij}/N^+}{\sum\limits_i n^-_{ij}/N^-}$ ratios of the normalized event distributions in Dalitz plots for $K^\pm \to \pi^\pm\pi^0\pi^0$ decays projected on the u' and $|v'|$ axes. The $r_{ij}(u')$ ratio versus u' for different $|v'|$ intervals are presented in Fig. 15.

Since some theoretical models predict that CP violation in $K^\pm \to 3\pi$ decays can be associated with the charge asymmetry of the slope g only, Δg is also estimated assuming $\Delta h = \Delta k = 0$ which is in agreement with (3). With this assumption we find:

$$\Delta g = 0.0002 \pm 0.0024 \qquad \chi^2/ndf = 319/(279-1) = 1.15. \tag{4}$$

The g, h, and k parameters appear to be equal for kaons of different signs within statistical uncertainties. But this does not guarantee the identity of the event distributions in the corresponding Dalitz plots. In order to check the identity of u', $|v'|$, and $(u', |v'|)$ distributions independently of the matrix element form (1), the Kolmogorov nonparametric criterion was used. This analysis provided the following results: the probabilities that u', $|v'|$ and two-dimensional $(u', |v'|)$ distributions for K^+ and K^- are indistinguishable are equal to 32.4%, 85.4% and 55.2% correspondingly. The two-dimensional $(u', |v'|)$ distributions were compared using the modified Kolmogorov criterion from the *HBOOK* code which works with histograms.

4.2 Systematic errors

All measures are taken to assure that K^+ and K^- beams have identical parameters. Nevertheless the average angles A_X and A_Y of beam particles with respect to the nominal beam axis and the mean kaon energies in the positive and negative beams could differ by $\Delta A_X = 5$ μrad, $\Delta A_Y = 7$ μrad and ΔE = 50 MeV. Simulations show that these uncertainties result in the following

systematic errors:

$$\delta_A(\Delta g) = 0.0004, \qquad \delta_A(\Delta h) = 0.0003, \qquad \delta_A(\Delta k) = 0.0001,$$
$$\delta_E(\Delta g) = 0.0006, \qquad \delta_E(\Delta h) = 0.0004, \qquad \delta_E(\Delta k) = 0.0001.$$

Two methods were used to evaluate systematic uncertainties of Δg, Δh, and Δk connected with g, h, k errors (see (2) and (A.1),(A.2) in Appendix): MC and the analytical method assuming ideal resolutions in u and v: $u \equiv u'$, $v \equiv v'$ (see (A.3),(A.4)). Both methods gave the same results:

$$\frac{\delta(\Delta g)}{\Delta g} \approx \sqrt{(0.2 \cdot \delta g)^2 + (0.6 \cdot \delta h)^2 + (1.6 \cdot \delta k)^2},$$
$$\frac{\delta(\Delta h)}{\Delta h} \approx \sqrt{(0.5 \cdot \delta g)^2 + (1.0 \cdot \delta h)^2 + (1.5 \cdot \delta k)^2},$$
$$\frac{\delta(\Delta k)}{\Delta k} \approx \sqrt{(0.4 \cdot \delta g)^2 + (0.5 \cdot \delta h)^2 + (2.9 \cdot \delta k)^2}.$$

Using experimental data [4] one can obtain:

$$\frac{\delta(\Delta g)}{\Delta g} = 0.014, \qquad \frac{\delta(\Delta h)}{\Delta h} = 0.024, \qquad \frac{\delta(\Delta k)}{\Delta k} = 0.019.$$

Other possible sources of the systematic errors include the time variations of the calorimeter calibration coefficients and the hodoscope efficiency, the influence of the Earth magnetic field on the particle beams of different polarity, the difference in the π^+ and π^-interactions with matter, and the difference in composition and intensity of the positive and negative beams. The total contribution of these factors to the systematic errors does not exceed $1 \cdot 10^{-4}$.

We also investigated that varying the minimum energy of γ's, the minimum and maximum energies of charged pion, the value of the χ^2 confidence level and the number of reconstructed tracks did not appreciably change the results. The results remain also unaffected if the bins located at the boundary of the Dalitz plot are not used. Δg, Δh, and Δk can also be found by minimizing the functional for the differences of the Dalitz plots. The obtained results agree with (3) and (4).

Thus, the final estimates of the systematic errors are

$$\delta(\Delta g) = 7 \cdot 10^{-4}, \qquad \delta(\Delta h) = 5 \cdot 10^{-4}, \qquad \delta(\Delta k) = 1.4 \cdot 10^{-4}. \tag{5}$$

The systematic errors are approximately an order of magnitude less than the statistical errors given in (3).

CONCLUSIONS

The differences Δg, Δh, Δk of the Dalitz plot parameters have been measured for the $K^{\pm} \to \pi^{\pm}\pi^0\pi^0$ decays using the TNF-IHEP facility. The studies were performed in the 35 GeV/c positive and negative hadron beams at the 70 GeV IHEP accelerator. Frequent changes of the beam polarity allow one to minimize the systematic uncertainties of the experiment. Our results show that the event distributions in the Dalitz plots for K^+ and K^- decays are indistinguishable and that the Δg, Δh, and Δk are equal to zero within the errors quoted (3),(5). Assuming $\Delta h = \Delta k = 0$ we find:

$$\Delta g = 0.0002 \pm 0.0024(stat.) \pm 0.0007(syst.).$$

To find $A_g = \Delta g/(g^+ + g^-)$ it is assumed $g^+ = g^- = 0.652$ [4]:

$$A_g = 0.0002 \pm 0.0018(stat.) \pm 0.0005(syst.).$$

This is the most accurate estimate of the charge asymmetry of the Dalitz plot slope for the $K^{\pm} \to \pi^{\pm}\pi^0\pi^0$ decay.

ACKNOWLEDGMENTS

We are grateful to A.A. Logunov, N.E. Tyurin, and A.M. Zaitzev for their support of the experiment; to V.N. Mikhailin for his assistance in the setup construction and operation; to Yu.V. Mikhailov, A.N. Sytin, and V.A.Sen'ko for their help in manufacturing electronics. We thank the staff of the Accelerator Department and the Beam Division who provided high-quality operations of the accelerator complex, beam extraction system, and the beam channels No.8 and No.23. We appreciate the assistance of I.N. Belyakov, Yu.G. Nazarov, A.N. Romadanov, and I.V. Shvabovich in the detector construction.

This study is supported in part by the Russian Fund for Basic Research (grants 02-02-17018, 02-02-17019) and the President grant 1305.2003.2.

APPENDIX

A Calculation of the differences of the Dalitz plot parameters

In accordance with (1), the probability density function can be expressed in the form:

$$f(u',v') = \frac{\int\limits_D G\cdot(1+gu+hu^2+kv^2)dudv}{\int\limits_D\int\limits_D G\cdot(1+gu+hu^2+kv^2)dudvdu'dv'},$$

where u, v and u', v' are the "true" and measured Dalitz variables, and $G \equiv G(u,v,u',v')$ is a function that depends on the efficiencies of the detectors and data processing. Integration is performed over the kinematic boundary of the Dalitz plot. This relation can be rewritten as:

$$f(u',v') = \frac{a+gb+hc+kd}{1+g\bar{u}+h\overline{u^2}+k\overline{v^2}},$$

where $a \equiv a(u',v') = \frac{1}{\varepsilon}\int\limits_D G\,dudv$, $b \equiv b(u',v') = \frac{1}{\varepsilon}\int\limits_D u\cdot G\,dudv$, $c \equiv c(u',v') = \frac{1}{\varepsilon}\int\limits_D u^2\cdot G\,dudv$, $d \equiv d(u',v') = \frac{1}{\varepsilon}\int\limits_D v^2\cdot G\,dudv$, $\bar{u} = \frac{1}{\varepsilon}\int\limits_D\int\limits_D u\cdot G\,dudvdu'dv'$, $\overline{u^2} = \frac{1}{\varepsilon}\int\limits_D\int\limits_D u^2\cdot G\,dudvdu'dv'$, and $\overline{v^2} = \frac{1}{\varepsilon}\int\limits_D\int\limits_D v^2\cdot G\,dudvdu'dv'$, and $\varepsilon = \int\limits_D\int\limits_D G\,dudvdu'dv'$. The $\bar{u}$, $\overline{u^2}$, and $\overline{v^2}$ are the mean values of the Dalitz variables and their squares, and ε is the total efficiency of the experiment (including the event reconstruction efficiency) for $|M|^2$=1.

Let's introduce the following notations:

$$g = (g^+ + g^-)/2, \qquad h = (h^+ + h^-)/2, \qquad k = (k^+ + k^-)/2,$$

$$\Delta g = g^+ - g^-, \qquad \Delta h = h^+ - h^-, \qquad \Delta k = k^+ - k^-.$$

Expanding the $\frac{f^+(u',v')}{f^-(u',v')}$ ratio of the normalized Dalitz plots into series in Δg, Δh, and Δk and neglecting their quadratic terms, we obtain

$$r(u',v') = \frac{f^+(u',v')}{f^-(u',v')} \approx 1+\alpha(u',v')\Delta g+\beta(u',v')\Delta h+\gamma(u',v')\Delta k, \quad \text{(A.1)}$$

where

$$\begin{aligned}
\alpha(u',v') &= [b - a\overline{u} + h(b\overline{u^2} - c\overline{u}) + k(b\overline{v^2} - d\overline{u})]/D(u',v'),\\
\beta(u',v') &= [c - a\overline{u^2} + g(c\overline{u} - b\overline{u^2}) + k(c\overline{v^2} - d\overline{u^2})]/D(u',v'),\\
\gamma(u',v') &= [d - a\overline{v^2} + g(d\overline{u} - b\overline{v^2}) + h(d\overline{u^2} - c\overline{v^2})]/D(u',v'),
\end{aligned} \tag{A.2}$$

$$D(u',v') = (1 + g\,\bar{u} + h\,\overline{u^2} + k\,\overline{v^2}) \cdot (a + g\,b + h\,c + k\,d).$$

In the case of $u' \equiv u$ and $v' \equiv v$, ("ideal" resolution) formulae (A.1),(A.2) have the form:

$$r_0(u,v) = 1 + \frac{A_0(u,v)\Delta g + B_0(u,v)\Delta h + C_0(u,v)\Delta k}{(1 + g\,\bar{u} + h\,\overline{u^2} + k\,\overline{v^2}) \cdot (1 + g\,u + h\,u^2 + k\,v^2)}, \tag{A.3}$$

where

$$\begin{aligned}
A_0(u,v) &= u - \overline{u} + h(u\overline{u^2} - u^2\overline{u}) + k(u\overline{v^2} - v^2\overline{u}),\\
B_0(u,v) &= u^2 - \overline{u^2} + g(u^2\overline{u} - u\overline{u^2}) + k(u^2\overline{v^2} - v^2\overline{u^2}),\\
C_0(u,v) &= v^2 - \overline{v^2} + g(v^2\overline{u} - u\overline{v^2}) + h(v^2\overline{u^2} - u^2\overline{v^2}).
\end{aligned} \tag{A.4}$$

References

[1] A. J. Bevan *et al.*, Phys. Lett. B465 (1999) 355.

[2] A. Lai *et al.*, Eur. Phys. J. C22 (2001) 231.

[3] A. Alavi–Harati *et al.*, Phys. Rev. Lett. 83 (1999) 22.

[4] K. Hagiwara et al., Phys. Rev. D66 (2002) 010001.

[5] A. A. Belkov *et al.*, Czech. J. Phys. 53 (2003) Suppl. A, hep–ph/0311209.

[6] G. D'Ambrosio *et al.*, Phys. Lett. B273 (1991) 497.

[7] G. Isidori *et al.*, Nucl. Phys. B381 (1992) 522.

[8] E. Gamiz, hep–ph/0401236 (2004).

[9] I. V. Ajinenko *et al.*, Phys. Lett. B567 (2003) 159.

[10] W. T. Ford *et al.*, Phys. Rev. Lett. 25 (1970) 1370.

[11] K. M. Smith *et al.*, Nucl. Phys. B91 (1975) 45.

[12] G. A. Akopdzhanov *et al.*, in Proceedings of the First International Workshop on Frontier Science — Charm, Beauty, and CP, Frascati, 2002, Ed. by L. Benussi *et al.* (LNF, Frascati, 2002), p. 229.

[13] V.V. Ammosov *et al.*, Preprint IHEP 98-2, Protvino, 1998.

[14] A.V. Vasiliev *et al.*, Instrum. Exp. Tech., 1993, vol. 2, p. 50.

[15] Yu.V. Gilitsky *et al.*, Preprint IHEP 93-10, Protvino, 1993.